

Article

Open Access



Novel “sandwich” configuration with ALD-coating layers on electrode/electrolyte interfaces for durable all-solid-state lithium metal batteries with high-voltage cathodes

Guohui Chen^{1,2}, Xiang Liu^{1,2}, Zewen Liu^{1,2}, Yun Zheng^{1,2,*}, Tianzhu Zhang^{1,2}, Farnood Rahmati³, Shuo Yan^{1,2}, Lanting Qian^{4,*}, Jie Dong⁵, Chunxiang Ma⁵, Shiyang Wei⁵, Wei Yan^{1,2}, Jiujun Zhang^{1,2,*}

¹College of Materials Science and Engineering, Institute of New Energy Materials and Engineering, Fuzhou University, Fuzhou 350108, Fujian, China.

²Fujian Engineering Research Center of High Energy Batteries and New Energy Equipment & Systems, Fuzhou University, Fuzhou 350108, Fujian, China.

³Electrochemical Technology Center, Department of Chemistry, University of Guelph, Guelph, ON N1G 2W1, Canada.

⁴Department of Chemical Engineering, University of Waterloo, Waterloo, ON N2L 3G1, Canada.

⁵Anhui Leoch Renewable Energy Development Co., Ltd, Huaibei 235000, Anhui, China.

***Correspondence to:** Prof. Yun Zheng, College of Materials Science and Engineering, Fuzhou University, No. 2, Xue Yuan Road, University Town, Fuzhou 350108, Fujian, China. E-mail: yunzheng@fzu.edu.cn; Lanting Qian, Departments of Materials Science and Engineering, University of Waterloo, 200 University Ave. W, Waterloo, ON N2L 3G1, Canada. E-mail: ltqian@uwaterloo.ca; Prof. Jiujun Zhang, College of Materials Science and Engineering, Fuzhou University, No. 2, Xue Yuan Road, University Town, Fuzhou 350108, Fujian, China. E-mail: jiujun.zhang@fzu.edu.cn

How to cite this article: Chen, G.; Liu, X.; Liu, Z.; Zheng, Y.; Zhang, T.; Rahmati, F.; Yan, S.; Qian, L.; Dong, J.; Ma, C.; Wei, S.; Yan, W.; Zhang, J. Novel “sandwich” configuration with ALD-coating layers on electrode/electrolyte interfaces for durable all-solid-state lithium metal batteries with high-voltage cathodes. *Energy Mater.* 2025, 5, 500064. <https://dx.doi.org/10.20517/energymater.2024.163>

Received: 7 Sep 2024 **First Decision:** 28 Nov 2024 **Revised:** 27 Dec 2024 **Accepted:** 8 Feb 2025 **Published:** 3 Mar 2025

Academic Editors: Yuping Wu, Federico Bella **Copy Editor:** Fangling Lan **Production Editor:** Fangling Lan

Abstract

Compositing inorganic ceramics and polymer materials to form all-solid-state electrolytes has been recognized as a feasible approach for the development of all-solid-state batteries. However, polymer-based electrolytes such as polyethylene oxide can electrochemically decompose above 3.9 V (vs. Li⁺/Li), which results in undesirable battery performance. Moreover, dendrite growth can occur on the anode side and further lead to battery short-circuit. This work designs and successfully fabricates stable electrode/electrolyte interfaces on both the composite cathode and anode sides after employing alucone coating layers made through atomic layer deposition. Due to the protection capability of such coating layers, the electrochemical degradation between the composite solid-state



© The Author(s) 2025. **Open Access** This article is licensed under a Creative Commons Attribution 4.0 International License (<https://creativecommons.org/licenses/by/4.0/>), which permits unrestricted use, sharing, adaptation, distribution and reproduction in any medium or format, for any purpose, even commercially, as long as you give appropriate credit to the original author(s) and the source, provide a link to the Creative Commons license, and indicate if changes were made.



electrolytes of $\text{Li}_7\text{La}_3\text{Zr}_2\text{O}_{12}$ /polyethylene oxide/lithium bis(trifluoromethane-sulfonyl) imide film and nickel-rich high voltage cathode ($\text{LiNi}_{0.8}\text{Mn}_{0.1}\text{Co}_{0.1}\text{O}_2$) has been obviously suppressed through the significantly improved anti-oxidation capability of the electrolyte. Simultaneously, the alucone coating layer can function as the protective barrier for the lithium metal anode, remarkably suppressing the growth of lithium dendrites. As a result, the obtained all-solid-state batteries with dual electrode/electrolyte interfaces show both high capacity retention and long cycle life, whereas the contrasting battery without protection coating layers shows both the fast capacity decay and micro-shortening behavior. This work presents an effective strategy for constructing more stable electrode/electrolyte interfaces for polymers-based all-solid-state batteries, and also provides a design rationale for materials and structure development in the field of energy storage and conversion.

Keywords: All-solid-state battery, lithium metal anode, atomic layer deposition, interface optimization, composite solid-state electrolyte, alucone

INTRODUCTION

High energy density batteries are essential for mobile applications, such as battery electric vehicles (BEVs) and plug-in hybrid vehicles (PHEVs), to realize smooth and efficient storage conversion for practical applications^[1-5]. Among different types of batteries, all-solid-state batteries (ASSBs) are deemed as one of the most promising technologies to achieve both high energy density and safety^[6-8]. For example, the Garnet-type solid-state electrolytes (SSEs)-based ASSBs are considered one of the most promising batteries due to relatively high ionic conductivity, wide electrochemical window, and excellent compatibility of SSEs with lithium (Li) metal anodes^[9-11]. However, a significant challenge arises from the substantial interfacial resistance between the garnet SSEs and electrode materials due to the inherent rigidity of their ceramic structure^[12]. The elevated interfacial resistance was also observed on the Li side because of the inadequate surface wetting characteristics and the formation of lithium carbonate impurities on their surfaces^[13-15]. Regarding this interfacial contact issue, incorporation of garnet SSEs into polymer electrolytes such as polyethylene oxide (PEO) to form composite SSEs (CSSEs) is recognized as an effective strategy, in which an intimate contact can be formed at the electrode/electrolyte interfaces to largely lower the interfacial resistance^[16,17].

Although CSSEs have shown good interface physical contact, their mechanical stability and electrochemical stability still need to be further improved with respect to the long-term cycling of batteries, even using the inorganic/polymer CSSE such as $\text{Li}_7\text{La}_3\text{Zr}_2\text{O}_{12}$ (LLZO)/PEO ones^[18]. To be specific, dendrite growth still can penetrate the CSSE from the anode side due to the low bulk and shear modulus of the polymer matrix such as PEO; thus, a uniform Li^+ plating to reduce dendrite growth is required for increasing long-term cycling of the battery^[19-21]. On the other hand, most polymer matrices tend to decompose at a relatively lower voltage; for example, the decomposition voltage of PEO is only 3.9 V (vs. Li^+/Li). Therefore, polymer-based CSSEs are generally limited to paired with lower voltage cathodes such as lithium iron phosphate (LFP). Furthermore, PEO also appears unsuitable when paired with the nickel-rich $\text{LiNi}_{0.8}\text{Mn}_{0.1}\text{Co}_{0.1}\text{O}_2$ (NCM811) cathode due to possible parasitic reactions, which can lead to significant performance degradation of the battery^[22-24].

To deal with the degradation issues of ASSBs, thin-film deposition techniques have been recognized as efficient methods for improving the electrode/electrolyte interface. For example, the coatings of Al_2O_3 , TiO_2 , ZrO_2 , ZnO and LiAlO_x through chemical vapor deposition (CVD), physical vapor deposition (PVD), and atomic layer deposition (ALD) have shown great effectiveness^[25,26]. Among these methods, ALD has stood out with its self-limiting feature, enabling precise modulation of sub-nanometer coatings, showing great potential for applications^[27,28]. In detail, ALD coatings can effectively mitigate the dissolution of

transition metals, minimize capacity loss at the cathode side, prevent interfacial side reactions, and improve the oxidative stability of the electrolyte^[29]. Moreover, the protection of lithium metal anodes (LMA) using ALD has shown effectiveness in facilitating lithium plating or acting as a physical barrier to constrain lithium dendrite^[30].

Regarding the ALD coating method, it has been extensively studied in liquid electrolyte-based batteries but has been less documented in ASSBs, especially for the above PEO-based ones^[31,32]. Besides, most of the reported research about ALD coating approaches for lithium batteries is focused on the anode or cathode side; the issues of anode/electrolyte interface and cathode/electrolyte interfaces have not sufficiently investigated simultaneously^[33,34]. In our opinion, a dual interface design via ALD in PEO-based ASSBs should be studied to well address both the issues of dendrite growth for inherent soft nature of PEO-based all-solid-state electrolytes (ASSEs) and the insufficient oxidation stability at a higher voltage. LLZO was selected as the ceramic solid electrolyte to combine with PEO in forming the CSSE because this system has been extensively studied in the literature and serves as an effective benchmark for comparing with our ALD-modified CSSE system.

In this work, a dual interface design via ALD in PEO-based ASSBs is proposed for the first time. In detail, a CSSE containing PEO, LLZO, and lithium bis (trifluoromethane-sulfonyl) imide (LiTFSI) (abbreviated as LLZO/PEO/LiTFSI) is successfully fabricated through a simple solvent casting method. One side of the cathode NCM811 and LMA is coated with an alucone thin layer using an ALD method. Then, the LLZO/PEO/LiTFSI electrolyte is sandwiched by both alucone thin layer-coated cathode and anode to form the ASSB (LMA-Alucone|LLZO/PEO/LiTFSI|Alucone-NCM811). Various advanced methods of representation show that the alucone-coated interfaces can prevent electrochemical degradation of the cathode side and facilitate lithium plating uniformly on the anode side. As a result, the assembled ASSB with the coated interfaces shows significantly improved cycling stability even at low external pressure (< 1 mPa). In comparison, the ASSB without ALD coating shows a significant capacity fade, and displayed micro-shorting behavior after only 80 cycles. Overall, the fabrication strategy of coating electrode/electrolyte interfaces through an ALD method in this work provides a new route to realize the robust interfaces in ASSBs, and sheds light on the development of durable devices in the area of energy storage and conversion.

EXPERIMENTAL SECTION

Fabrication of the CSSE

Commercially available 99.99% purity LLZO with an average particle size of 500 nm was purchased from MTI Corp. PEO (Mn = 400,000), LiTFSI and other common chemicals were purchased from Sigma-Aldrich Inc. In the preparation of the CSSE, PEO and LiTFSI were weighed at a molecular ratio of 16:1, and further dissolved in acetonitrile in the glovebox overnight to form a mixture. Then, LLZO powder was dissolved into this mixture and stirred overnight. The obtained mixture was then cast onto the custom-made Teflon plate (with film size desired) to form a film, which was slowly dried at 80 °C to obtain the final CSSE (marked as LLZO/PEO/LiTFSI in this work, where the individual component mass ratio is 35:50:32). The obtained thickness and diameter of the LLZO/PEO/LiTFSI film were about 100 μm and 18 mm, respectively.

Cathode preparation and ALD coating

Cathode components of NCM811, Super-P, and polyvinylidene fluoride (PVDF) were mixed in a mass ratio of 90%, 5%, and 5%, respectively, and then pulverized with a high-shear mixer with the addition of N-Methylpyrrolidone (NMP) solvent to make a homogeneous slurry. This cathode slurry was cast onto an aluminum current collector using a doctor blade, which was then dried under vacuum at 90 °C for 24 h.

Subsequently, the coated cathode was sectioned into 12 mm diameter discs for alucone coating using ALD methods. The cathode alucone coating layer using the ALD method was deposited at 100 °C by introducing trimethylaluminum (TMA) and ethylene glycol into an ALD reactor (PALD-150D, China). The thickness of the alucone coating layer on the cathode NCM811 surface was about 2 nm.

Lithium metal anode coating using alucone by ALD

The alucone coating through ALD methods for LMA (diameter 15.6 mm) followed the same procedure as the cathode coating. The thickness of the alucone coating layer on the LMA surface was about 2 nm. The entire process was conducted inside a glovebox in an argon environment.

Characterizations

Powder X-ray diffraction (XRD) measurements were performed on all materials using Cu-K α radiation (Bruker, D8 Advance, Germany). The morphology of uncoated and ALD-coated NCM811 powder was analyzed using a field emission scanning electron microscope (SEM) (LEO Zeiss 1550, Switzerland), while elemental distribution was assessed through energy-dispersive X-ray spectroscopy (EDS). Elemental contents and valence states of the samples were analyzed using Thermo Fisher Scientific's K-Alpha X-ray photoelectron spectroscopy (XPS) equipment, and the XPS system was equipped with dual turbo molecular pumps, a monochromatic micro-focused low-power Al K-Alpha X-ray source, and a 128-channel detector, to achieve efficient data acquisition.

A depth profile analysis was performed utilizing the time-of-flight secondary ion mass spectrometry (TOF-SIMS) technique, employing the TOF-SIMS 5-100 instrument from ION-TOF GmbH, Germany. X-ray adsorption spectroscopy (XAS) experiments were conducted at the BL14W1 beamline of the Shanghai Synchrotron Radiation Facility (SSRF), utilizing Co K-edge X-rays. Ni L-edge experiment was conducted on the BL12B beamline at the State Key Laboratory of Synchrotron Radiation at the University of Science and Technology of China, Hefei 230029, China. The pair distribution function analysis (PDF) was performed using an EMPYREAN X-ray diffractometer with Ag target (Netherlands, Malvern Panalytical).

Cell assembly

Both working and counter electrodes were Li plates for a Li-Li symmetrical cell, which was assembled into a CR2032-type coin cell using the as-prepared CSSE in a glove box filled with argon, maintaining both water and oxygen levels below 0.5 ppm. Similarly, the full cell was assembled with pristine or alucone-coated LMA, CSSE, and alucone-coated or alucone-free NCM811 cathode in an Ar-filled glove box to form full cells (LMA-Alucone|LLZO/PEO/LiTFSI|Alucone-NCM811, or LMA|LLZO/PEO/LiTFSI|NCM 811). The external pressure is typical of the spring force applied (~100 kPa). It should be noted that no liquid electrolyte was added into the assembled cells.

Electrochemical measurements

The electrochemical impedance spectroscopy (EIS) test was conducted by using the Biologic multi-channel electrochemical workstation with a frequency range of 100 mHz to 100 kHz and an AC amplitude of 10 mV. The method for calculating ionic conductivity was included in the [Supplementary Material](#).

The electrochemical performance test was performed for the assembled coin cell after resting for 12 h. A VMP3 (Bio-Logic) battery cycler was used to measure the electrochemical performance of the symmetrical and full cells. The performance of lithium metal batteries with NCM811 as the cathode was tested with a voltage range from 2.8 to 4.3 V.

RESULTS AND DISCUSSION

Structural analysis of the ASSB with dual interface design

The structure of the proposed ASSB with dual interface design is presented in [Figure 1](#). It can be seen that the ASSB has a “sandwich” configuration and the thin layers of alucone are coated on both the cathode and anode surfaces. The purpose of the alucone coating layers is to prevent electrochemical degradation reactions between the CSSE of LLZO/PEO/LiTFSI and NCM811 cathode, as well as the side reactions between the CSSE and LMA.

ALD was carried out with 15 cycles of deposition, resulting in a thickness of alucone coating layer of ~2 nm. The coated cathode is depicted in [Figure 1B](#), which shows that the active material is uniformly distributed and protected by the coated alucone layer. A SEM image of the NCM811 cathode without alucone coating is presented for comparative analysis, as shown in [Supplementary Figure 1](#). Similarly, LMA is coated with the same material, as revealed by the SEM image in [Figure 1C\(i\)](#), and EDS data in [Figure 1C\(ii\)](#) and [\(iii\)](#), which indicates a uniform ALD coating of alucone. The coin cell-shaped CSSE film is composed of PEO, LLZO and LiTFSI in a mixed matrix as shown in [Figure 1D](#) and [E](#). It can be seen that the film is uniform and flexible, and its mechanical properties can be favorable for enabling low-pressure cells with good wettability.

Both the chemical environment and molecular interactions in the critical components including LLZO/PEO/LiTFSI film and alucone-coated NCM811 cathode were further investigated by XPS and XAS. In detail, XPS was used to characterize the LLZO/PEO/LiTFSI film and understand how LiTFSI was dissolved into the material, as shown in [Figure 2A-D](#). All XPS spectra were calibrated and corrected based on adventitious carbon. The C 1s signal shows a typical PEO structure with CH₂- and (-OCH₂-CH₂)_n groups at ~284.8 and 286.6 eV, and CF₃ functionality at ~293.0 eV [[Figure 2A](#)], which indicates that the LiTFSI has broken down and reacted with the carbon atoms from the PEO^[35]. This is also supported by the S 2p and F 1s XPS data, namely the peaks of CF₃ (688.7 eV), LiF (685.2 eV), LiTFSI (168.9 and 170.1 eV), and Li_xS_yO_z (167.1 and 168.3 eV), which show the dissociation of lithium salt [[Figure 2B](#) and [C](#)], and this is also confirmed by the Li 1s XPS as displayed in [Supplementary Figure 2](#)^[36]. In the O 1s signal [[Figure 2D](#)], the presence of C-O bonds is observed, which aids in the formation of a stable and structurally ordered solid electrolyte interphase (SEI) layer on the electrode surface. The formed SEI layer enhances its structural stability by forming hydrogen bonds or electrostatic interactions with the ions from the electrolyte^[37]. The dissociation of lithium salt could also subsequently facilitate the reduction of Li⁺-TFSI⁻ pairs towards much more liberated Li⁺, further promoting the migration and transformation of lithium^[38].

In addition to the structural analysis for LLZO/PEO/LiTFSI film by XPS, the cathode side with or without an alucone coating layer was detected through XAS, which included both X-ray absorption near edge structure (XANES) and extended X-ray absorption fine structure (EXAFS) sections and was very informative on both the oxidation and coordination states of metal species^[39]. Specifically, the XAS results of the alucone-coated and pristine NCM811, along with their k³-weighted R space transformation, are displayed in [Figure 2E](#) and [F](#). The absorption energy (E₀) of the Co K-edge slightly shifts to higher energy, indicating that the alucone coating can slightly alter the surface status of NCM811. The slight shift to higher E₀ is likely due to the Al-O-Co bonding, causing the Co to be more electron deficient^[40,41]. This is further verified in the R space of the XAS spectra [[Figure 2F](#)], which shows slight bonding changes, particularly at ~1 Å, indicating the change of Co-O bonding^[42,43].

As observed, the alucone-coated cathode tends to show a slightly lower electronic conductivity than the pristine one without coating, which stems from the electronically insulating nature of the alucone, while the ionic conductivity stays more or less the same. This is because the alucone layer is sufficiently thin, which

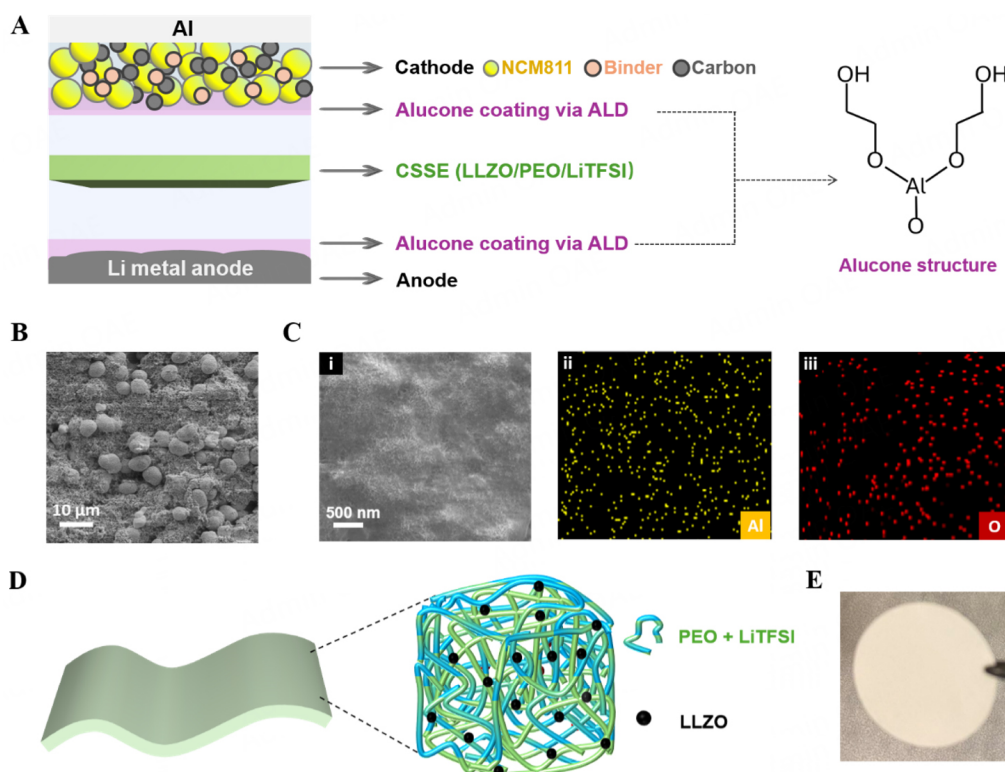


Figure 1. Structure of the proposed dual interface design in ASSBs. (A) Schematic representation of a “sandwich” dual protection on LMA and NCM811 cathode. (B) SEM image of the alucone coated NCM811 cathode. (C) SEM image (i) and EDS mapping of the alucone coating on LMA: Al element (ii) and O element (iii). (D) Schematics of LLZO/PEO/ LiTFSI film made of PEO, LLZO and LiTFSI. (E) Fabricated LLZO/PEO/LiTFSI film with a diameter of 18 mm.

does not much alter the ionic conductivity. As shown in [Supplementary Figure 3](#), the ionic conductivity (σ) of the LLZO/PEO/LiTFSI film is $1.28 \times 10^{-4} \text{ S cm}^{-1}$ through the ionic conductivity test at 50 °C. Therefore, the balance between electrochemical performance and interfacial protection can be maintained when performing with this ALD coating strategy.

Electrochemical performance of lithium metal anode

Initially, the Li-Li symmetric cells were assembled to illustrate the impact of the alucone coating layer on the interface stability between LMA and LLZO/PEO/LiTFSI films. [Figure 3A](#) shows the cyclic testing on the cells of LMA|PEO/LiTFSI|LMA, LMA|LLZO/PEO/LiTFSI|LMA, and LMA-Alucone|LLZO/PEO/LiTFSI|Alucone-LMA under a current density of 0.1 mA cm^{-2} and a surface capacity of 0.1 mAh cm^{-2} . The results reveal that the originally assembled LMA|PEO/LiTFSI|LMA cell exhibits a significant interface resistance due to the inadequate interface contact which results in considerable polarization voltage and unstable performance during cycling. The LMA|LLZO/PEO/LiTFSI|LMA cell can improve interface contact a bit, but the non-uniform deposition sites can lead to premature core short-circuit, indicating that enhancing stability of the interface solely through composite electrolyte construction is insufficient^[44]. In comparison, the LMA-Alucone|LLZO/PEO/LiTFSI|Alucone-LMA cell demonstrates a consistent cycling performance, validating that the alucone coating layer can not only enhance the electrode/electrolyte interface but also promote uniform lithium deposition. Additionally, as illustrated by the magnified view at the end of cycling in [Figure 3B](#), alucone coating layers on the electrode interface can also reduce the polarization voltage ($< 50 \text{ mV}$) during cycling. These results above suggest that integrating an alucone coating layer onto a LLZO/PEO/LiTFSI film can optimize interface contact and enhance the stability of the interface as well.

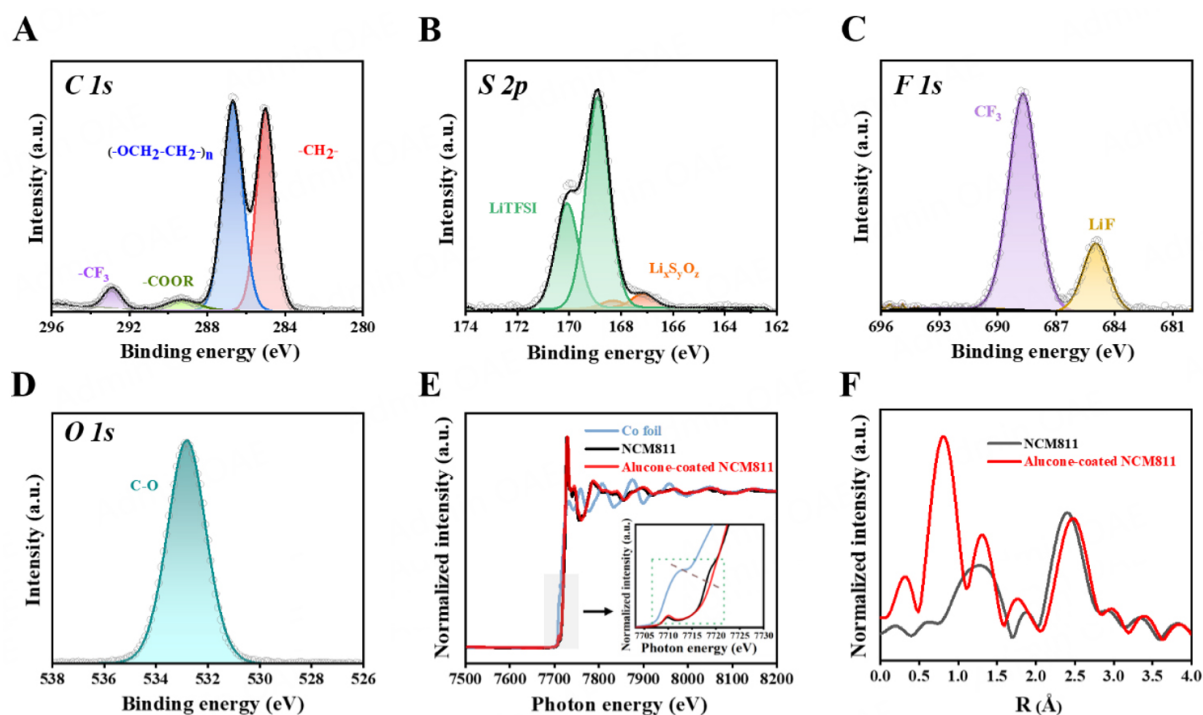


Figure 2. Chemical environment and molecular interactions. (A) C1s, (B) S2p, (C) F1s, (D) O1s XPS spectra of the LLZO/PEO/LiTFSI film. (E) Co K-edge XANES spectra (energy space) of NCM811 and the alucone-coated NCM811 cathodes, and (F) magnitude of k^3 -weighted Fourier transforms of EXAFS spectra (R space transformation).

Aside from the stability of cycling on the Li-Li symmetric cells, the morphological changes of the LMA surface following Li stripping and plating over 100 cycles were also examined. As depicted in [Figure 3C](#), the LMA from LMA|LLZO/PEO/LiTFSI|LMA displays a rough and porous interface after cycling, characterized by numerous fern-like Li dendrites. In comparison, the LMA from LMA-Alucone|LLZO/PEO/LiTFSI|Alucone-LMA, as illustrated in [Figure 3D](#), exhibits a smoother and more compact surface texture with only some coarse and short protrusions. The SEM images offer a clear visual comparison between the LMA interfaces from LMA|LLZO/PEO/LiTFSI|LMA and LMA-Alucone|LLZO/PEO/LiTFSI|Alucone-LMA highlighting the substantial disparity in their interfaces and demonstrating the inhibitory effect of the alucone coating layer on side reactions and lithium dendrite growth^[45]. For further study, TOF-SIMS was also used to observe the element distribution at the interfaces, as illustrated in [Figure 3E-H](#). The 2D mapping of CH_x^- and COO^- signals reveals a much higher intensity on the surface of LMA|LLZO/PEO/LiTFSI|LMA than that in LMA-Alucone|LLZO/PEO/LiTFSI|Alucone-LMA, in which the black regions reveal the absence of signal, possibly stemming from the decomposition of PEO and the reaction with LMA^[46,47]. This finding further validates that the alucone-coated layer by ALD can effectively mitigate the reactivity between LMA and the electrolyte, thereby averting the electrolyte decomposition^[48].

Electrochemical performance of full-cell with dual interface design

In addition to evaluating the electrochemical performance of alucone-coated LMA and the NCM811 cathode, the full-cell ASSB that contained both alucone-coated LMA and NCM811 cathode with LLZO/PEO/LiTFSI as the electrolyte (LMA-Alucone|LLZO/PEO/LiTFSI|Alucone-NCM811) was assembled and its performance was investigated by electrochemical methods. [Figure 4A](#) shows the cycle stability (performed at 0.1C at 50 °C) comparison between the LMA|LLZO/PEO/LiTFSI|NCM811 and LMA-Alucone|LLZO/PEO/LiTFSI|Alucone-NCM811 batteries. In the former case, the battery shows a constant

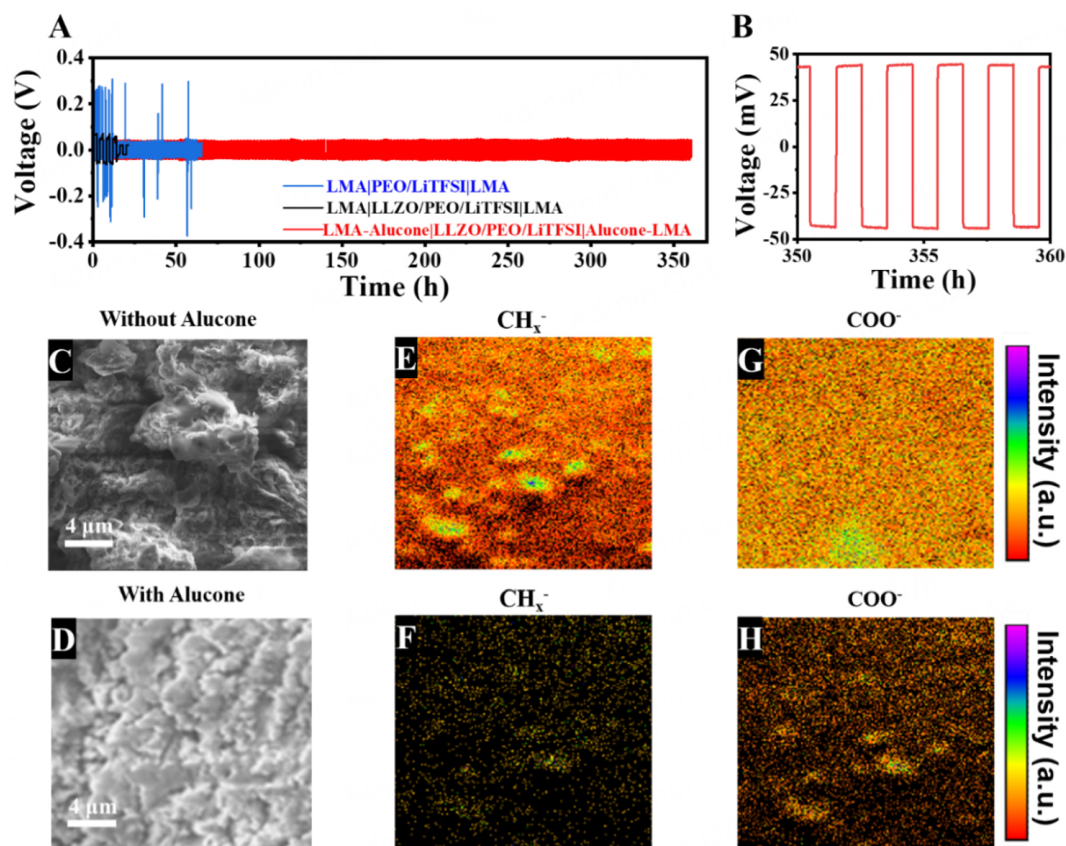


Figure 3. Characteristics for Li-Li symmetric cells: (A) Cycling performance comparison among Li/Li symmetric cells using different electrolytes (PEO/LiTFSI or LLZO/PEO/LiTFSI) and different Li metal electrode (with or without alucone coating layer by ALD method); (B) Enlarged view showing cycling performance of LMA-Alucone|LLZO/PEO/LiTFSI|Alucone-LMA in (A). SEM images depicting the morphologies on the surface of LMA after 100 cycles from (C) LMA|LLZO/PEO/LiTFSI|LMA and (D) LMA-Alucone|LLZO/PEO/LiTFSI|Alucone-LMA. TOF-SIMS 2D mapping on the surface of LMA after cycling: signals of CH_x^- from (E) LMA|LLZO/PEO/LiTFSI|LMA and (F) LMA-Alucone|LLZO/PEO/LiTFSI|Alucone-LMA, as well as signals of COO^- from (G) LMA|LLZO/PEO/LiTFSI|LMA and (H) LMA-Alucone|LLZO/PEO/LiTFSI|Alucone-LMA.

capacity fading; this resulted from the electrochemical degradation reactions between NCM811 and the LLZO/PEO/LiTFSI. In comparison, the latter demonstrates a much higher reversible capacity at ~ 175 mAh/g with negligible capacity fade in the first 80 cycles [Figure 4A and B]. The LMA-Alucone|LLZO/PEO/LiTFSI|Alucone-NCM811 battery can retain $\sim 84\%$ of its initial capacity after 200 cycles at 0.1C. In comparison, the LMA|LLZO/PEO/LiTFSI|NCM811 battery can only retain 44% of its initial capacity with micro-shortening behavior after 80 cycles [Figure 4B]. Aside from the electrochemical measurements at 50 °C, the cycling performance of LMA-Alucone|LLZO/PEO/LiTFSI|Alucone-NCM811 at 0.2C at room temperature is shown in Supplementary Figure 4.

In addition, the average Coulombic efficiency (CE) of the battery without alucone coating layers shows 98.2% compared to 99.9%. The lower CE can result from continuous parasitic reactions likely at the cathode side, whereas the excess Li^+ should not contribute to the lowered CE^[49]. On the anode side, the CE is boosted by the excess Li. The battery was cycled at 0.1C rate due to the more prominent decomposition at lower C rate, which is better for comparison in this study. As shown in Figure 4C and D, when the battery is operated at different rates, the result demonstrates excellent rate performance compared to previous works^[50-52], due to the following two aspects: first, the alucone coating layers can improve the stability of the

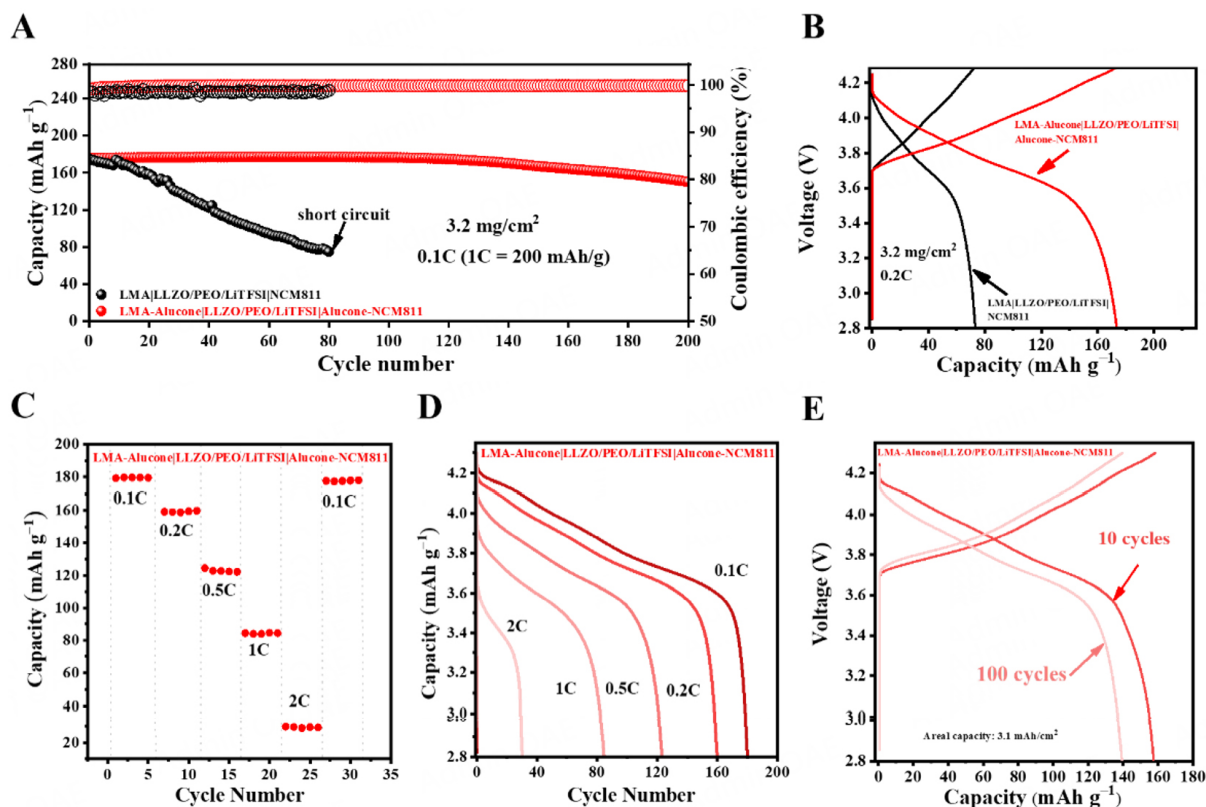


Figure 4. Electrochemical performance of full-cell with dual interface design. (A) Comparison of cycling data of LMA|LLZO/PEO/LiTFSI|NCM811 and LMA-Alucone|LLZO/PEO/LiTFSI|Alucone-NCM811 batteries cycled at 50 °C. (B) The associated charge and discharge curves after 80 cycles. Performance of LMA-Alucone|LLZO/PEO/LiTFSI|Alucone-NCM811 battery: (C) specific capacity from 0.1C to 2C, at 50 °C; (D) discharge voltage profiles from 0.1C to 2C; (E) charge/discharge voltage profiles with an areal capacity of 3.1 mAh cm⁻².

electrode/electrolyte interfaces; second, such coating layers can optimize the contact at the interface and improves ion diffusion. Since the capacity of the LMA|LLZO/PEO/LiTFSI|NCM811 battery is constantly fading, reliable rate performance over stable cycles cannot be established. To be competitive with commercial lithium-ion batteries, the LMA-Alucone|LLZO/PEO/LiTFSI|Alucone-NCM811 battery with an areal capacity of 3.1 mAh cm⁻² (mass loading of NCM811 is ~20 mg cm⁻²) was constructed, which showcased an excellent performance with the alucone-coated LMA and NCM811 in Figure 4E. The battery demonstrated an initial capacity of ~180 mAh/g and retained 87% of its capacity at 0.1C after 100 cycles.

Origin of the enhanced performance induced by ALD strategy

To understand the protection mechanism of the alucone coating layer, EIS was conducted to check the interfacial resistance of the LMA|LLZO/PEO/LiTFSI|NCM811 and LMA-Alucone|LLZO/PEO/LiTFSI|Alucone-NCM811 batteries after 50 cycles [Figure 5A]. The battery without alucone coating layers shows a resistance of 607 Ω, whereas the resistance of the battery with coating only showed 152 Ω. This result indicates that the interfacial resistance induced by the electrochemical degradation has been much more severe in the LMA|LLZO/PEO/LiTFSI|NCM811 battery compared to LMA-Alucone|LLZO/PEO/LiTFSI|Alucone-NCM811 batteries, which is consistent with the rapid capacity fading seen in Figure 4A. The EIS spectra were fitted with a transmission line model documented elsewhere^[53,54].

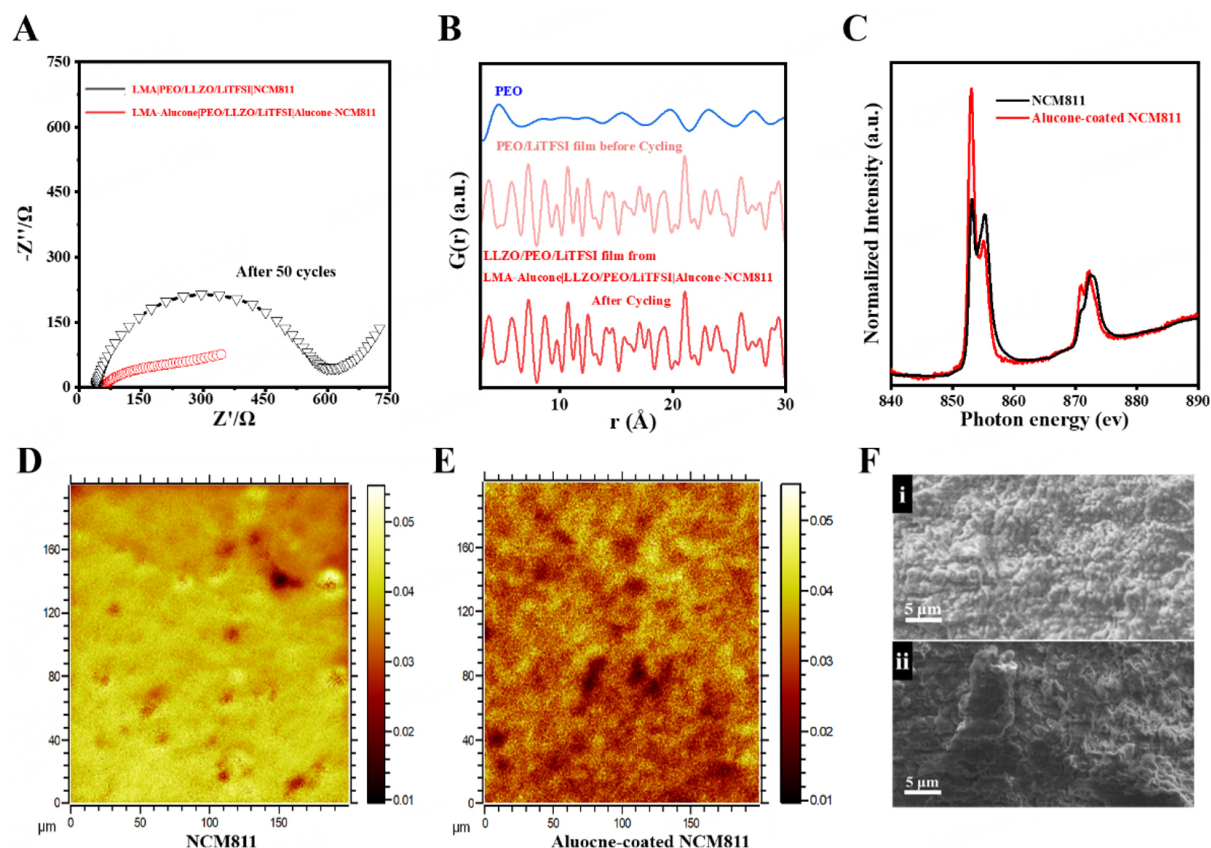


Figure 5. Origin of the enhanced performance enabled by ALD strategy. (A) Comparison of EIS spectra of LMA-Alucone|LLZO/PEO/LiTFSI|Alucone-NCM811 and LMA|LLZO/PEO/LiTFSI|NCM811 batteries after 50 cycles at 0.1C, 50 °C. (B) PDF of the LLZO/PEO/LiTFSI film before and after cycling in the LMA-Alucone|LLZO/PEO/LiTFSI|Alucone-NCM811 battery. (C) XAS of Ni L-edge of NCM811 (without ALD coating) and alucone-coated NCM811 cathodes. Normalized COO⁻ signal from TOF-SIMS on the surface of (D) NCM811 and (E) alucone-coated NCM811 cathodes after cycling. (F) SEM images of Li metal surface after 50 cycles of the (i) LMA-Alucone|LLZO/PEO/LiTFSI|Alucone-NCM811 battery and (ii) LMA|LLZO/PEO/LiTFSI|NCM811 battery.

PDF, XAS, ToF-SIMS and SEM were further employed to check the interfacial products for those two batteries on the cycled cathodes. The purpose of these characterization is to see if there is any damage to the NCM811 from cathode reaction or lithium dendrite growth to the electrolyte. The PEO portion of the LLZO/PEO/LiTFSI film from the battery with alucone coating layer is known to be amorphous, at which normal XRD cannot detect any diffuse scattering. Therefore, to examine the potential bonding of LLZO/PEO/LiTFSI film with the alucone coating layer, the total scattering experiment coupled with PDF was used. The result of PDF also shows negligible changes to the LLZO/PEO/LiTFSI film in LMA-Alucone|LLZO/PEO/LiTFSI|Alucone-NCM811 batteries [Figure 5B], which indicates that the LLZO/PEO/LiTFSI is successfully preserved due to the functional role of the alucone coating layer.

The cathode materials were disassembled from the batteries and subject to XAS characterizations. Figure 5C shows the Ni L-edge of the cathodes from LMA|LLZO/PEO/LiTFSI|NCM811 and LMA-Alucone|LLZO/PEO/LiTFSI|Alucone-NCM811 batteries. The valence state of Ni can be evaluated by the ratio of the peaks located at ~852 and 856 eV. Higher ratio of the peaks of alucone-coated NCM811 after cycling indicates the low oxidation of Ni in the pristine NCM811^[55,56]. In comparison, the cycled LMA|LLZO/PEO/LiTFSI|NCM811 battery shows a much lower ratio of the peaks which indicates that Ni has been partially oxidized due to the cycling^[57].

Furthermore, TOF-SIMS was used to understand the degradation products such as oxidized COO⁻ functional group as a result of PEO being oxidized. Figure 5D and E displays the normalized COO⁻ signal on the surface of NCM811 cathodes without or with alucone coating layers after cycling. Clearly, the intensity of COO⁻ signals for the alucone-coated NCM811 is much less than that of the NCM811 without coating layers, indicating that the oxidative decomposition of PEO is suppressed^[58]. On the anode side, LMA was peeled and subjected to microscopy measurements. Figure 5F(i) and (ii) shows the SEM images of LMA surfaces from the cycled batteries with or without alucone coating layers, respectively. The LMA surface from the battery with alucone coating layer shows a much more compact morphology in comparison to that from the battery without alucone coating layer. By comparison, the LMA surface from the battery without an alucone coating layer shows protrusions and aggregates because of the localized lithium plating. The better lithium plating in the battery of LMA-Alucone|LLZO/PEO/LiTFSI|Alucone-NCM811 can be attributed to both physical constraint and lithiophilic behavior of the alucone coating layer, which may be similar to the Al₂O₃ as discussed in previous publications^[59-61].

CONCLUSIONS

In this work, a “sandwich” configuration of a dual interface design is proposed to simultaneously protect the cathode and anode sides in ASSBs. The thickness of the alucone coating layers through ALD methods can be tuned at the nano-meter scale; such sufficiently thin coating layers can protect the batteries without suffering the drawbacks of lowered ionic conductivity. A combination characterization of several advanced techniques shows that the oxidative decomposition of the CSSE film of LLZO/PEO/LiTFSI is effectively suppressed, which enables a significant enhancement in the battery performance, and the short-circuit is prevented due to more uniform lithium plating on the anode side. As a result, the obtained LMA-Alucone|LLZO/PEO/LiTFSI|Alucone-NCM811 battery demonstrates a capacity retention of 84% after cycling for 200 cycles at 0.1C, whereas the contrast cell without protection from the alucone coating layers shows both fast capacity fading and micro-shortening behavior after 80 cycles. This work demonstrates the importance of dual interface protection of using a much less explored ALD coating technique for alucone coating layers for inorganic/organic CSSE-based ASSBs.

DECLARATIONS

Acknowledgments

The authors would like to acknowledge the financial support from the Natural Science Foundation of Fujian Province, the Educational Research Projects for Young and Middle-aged Teachers in Fujian Province, Fuzhou University Testing Fund of Precious Apparatus, the National Natural Science Foundation of China, Pilot Group Program of the Research Fund for International Senior Scientists, the Fujian Province Super 100 Talents Program, Fujian Province 100 Talents Program, Fujian Province Minjiang Scholar Program, and the Institute of New Energy Materials and Engineering, College of Materials Science and Engineering, Fuzhou University, First-Class Discipline Training Project. The authors also acknowledge Yi Cui, Yaping Kong, Rong Huang, and Nan Hu for the TOF-SIMS characterizations at the Vacuum Interconnected Nanotech Workstation (Nano-X, C24012), Suzhou Institute of Nano-Tech and Nano-Bionics, Chinese Academy of Sciences. Lastly, the authors wish to acknowledge the anonymous reviewers who provided a lot of helpful suggestions to enhance this article.

Authors' contributions

Methodology, investigation, and manuscript writing: Chen, G.; Liu, X.; Liu, Z.; Qian, L.; Zheng, Y.; Dong, J.; Ma, C.; Wei, S.

Performed data acquisition: Chen, G.; Liu, X.; Liu, Z.; Zhang, T.; Rahmati, F.; Yan, S.

Project administration and funding acquisition: Zheng, Y.; Zhang, J.

Conceptualization and supervision: Zheng, Y.; Zhang, J.; Yan, W.

Availability of data and materials

The data supporting this work are provided in the [Supplementary Materials](#). Additional raw data will be made available by the authors upon request.

Financial support and sponsorship

This work was funded by the Natural Science Foundation of Fujian Province (2024J01261), the financial support from the the Educational Research Projects for Young and Middle-aged Teachers in Fujian Province (JZ230002), Fuzhou University Testing Fund of Precious Apparatus (2024T010), the National Natural Science Foundation of China, Pilot Group Program of the Research Fund for International Senior Scientists (22250710676), the Fujian Province Super 100 Talents Program, Fujian Province 100 Talents Program, Fujian Province Minjiang Scholar Program, and the Institute of New Energy Materials and Engineering, College of Materials Science and Engineering, Fuzhou University, First-Class Discipline Training Project.

Conflict of interests

All authors declared that there are no conflicts of interest.

Ethical approval and consent to participate

Not applicable.

Consent for publication

Not applicable.

Copyright

© The Author(s) 2025.

REFERENCES

1. Xing, J.; Bliznakov, S.; Bonville, L.; Oljaca, M.; Maric, R. A review of nonaqueous electrolytes, binders, and separators for lithium-ion batteries. *Electrochem. Energy. Rev.* **2022**, *5*, 131. [DOI](#)
2. Zheng, Y.; Chen, Z.; Zhang, J. Solid oxide electrolysis of H₂O and CO₂ to produce hydrogen and low-carbon fuels. *Electrochem. Energy. Rev.* **2021**, *4*, 508-17. [DOI](#)
3. Or, T.; Gourley, S. W. D.; Kaliyappan, K.; Zheng, Y.; Li, M.; Chen, Z. Recent progress in surface coatings for sodium-ion battery electrode materials. *Electrochem. Energy. Rev.* **2022**, *5*, 137. [DOI](#)
4. Zhang, Z.; Zhang, H.; Wu, Y.; et al. Advances in doping strategies for sodium transition metal oxides cathodes: a review. *Front. Energy.* **2024**, *18*, 141-59. [DOI](#)
5. Shang, Z.; Li, T.; Hu, B.; et al. Two-dimensional bimetallic selenium-containing metal-organic frameworks and their calcinated derivatives as electrocatalysts for overall water splitting. *Front. Energy.* **2024**, *18*, 378-89. [DOI](#)
6. Li, Q.; Sun, X.; Cao, D.; Wang, Y.; Luan, P.; Zhu, H. Versatile electrospinning for structural designs and ionic conductor orientation in all-solid-state lithium batteries. *Electrochem. Energy. Rev.* **2022**, *5*, 170. [DOI](#)
7. Qian, L.; Singh, B.; Yu, Z.; et al. Unlocking lithium ion conduction in lithium metal fluorides. *Matter* **2024**, *7*, 3587-607. [DOI](#)
8. Wang, H.; Duan, S.; Zheng, Y.; et al. Solid-state electrolytes based on metal-organic frameworks for enabling high-performance lithium-metal batteries: fundamentals, progress, and perspectives. *eTransportation* **2024**, *20*, 100311. [DOI](#)
9. Wang, C.; Fu, K.; Kammampata, S. P.; et al. Garnet-type solid-state electrolytes: materials, interfaces, and batteries. *Chem. Rev.* **2020**, *120*, 4257-300. [DOI](#)
10. Feng, X.; Fang, H.; Wu, N.; et al. Review of modification strategies in emerging inorganic solid-state electrolytes for lithium, sodium, and potassium batteries. *Joule* **2022**, *6*, 543-87. [DOI](#)
11. Janek, J.; Zeier, W. G. Challenges in speeding up solid-state battery development. *Nat. Energy.* **2023**, *8*, 230-40. [DOI](#)
12. Yu, S.; Schmidt, R. D.; Garcia-mendez, R.; et al. Elastic properties of the solid electrolyte Li₇La₃Zr₂O₁₂ (LLZO). *Chem. Mater.* **2016**, *28*, 197-206. [DOI](#)

13. Xian, C.; Zhang, S.; Liu, P.; et al. An advanced gel polymer electrolyte for solid-state lithium metal batteries. *Small* **2024**, *20*, e2306381. DOI
14. Tu, Q.; Shi, T.; Chakravarthy, S.; Ceder, G. Understanding metal propagation in solid electrolytes due to mixed ionic-electronic conduction. *Matter* **2021**, *4*, 3248-68. DOI
15. Singh, D. K.; Fuchs, T.; Krempaszky, C.; et al. Origin of the lithium metal anode instability in solid-state batteries during discharge. *Matter* **2023**, *6*, 1463-83. DOI
16. Wan, J.; Wan, M.; Hou, X.; et al. Combining ternary, ionic liquid-based, polymer electrolytes with a single-ion conducting polymer-based interlayer for lithium metal batteries. *Energy Mater.* **2024**, *4*, 400074. DOI
17. Xiao, Y.; Wang, Y.; Bo, S.; Kim, J. C.; Miara, L. J.; Ceder, G. Understanding interface stability in solid-state batteries. *Nat. Rev. Mater.* **2020**, *5*, 105-26. DOI
18. Zheng, Y.; Yao, Y.; Ou, J.; et al. A review of composite solid-state electrolytes for lithium batteries: fundamentals, key materials and advanced structures. *Chem. Soc. Rev.* **2020**, *49*, 8790-839. DOI
19. Shi, C.; Song, J.; Zhang, Y.; et al. Revealing the mechanisms of lithium-ion transport and conduction in composite solid polymer electrolytes. *Cell. Rep. Phys. Sci.* **2023**, *4*, 101321. DOI
20. Zhao, X.; Wang, C.; Liu, H.; Liang, Y.; Fan, L. A review of polymer-based solid-state electrolytes for lithium-metal batteries: structure, kinetic, interface stability, and application. *Batteries. Supercaps.* **2023**, *6*, e202200502. DOI
21. Yang, L.; Nie, Y.; Liu, Y.; et al. The plasticizer-free composite block copolymer electrolytes for ultralong lifespan all-solid-state lithium-metal batteries. *Nano. Energy.* **2022**, *100*, 107499. DOI
22. Zhou, W.; Wang, S.; Li, Y.; Xin, S.; Manthiram, A.; Goodenough, J. B. Plating a dendrite-free lithium anode with a polymer/ceramic/polymer sandwich electrolyte. *J. Am. Chem. Soc.* **2016**, *138*, 9385-8. DOI
23. Yang, X.; Jiang, M.; Gao, X.; et al. Determining the limiting factor of the electrochemical stability window for PEO-based solid polymer electrolytes: main chain or terminal -OH group? *Energy Environ. Sci.* **2020**, *13*, 1318-25. DOI
24. Duan, S.; Qian, L.; Zheng, Y.; et al. Mechanisms of the accelerated Li^+ conduction in MOF-based solid-state polymer electrolytes for all-solid-state lithium metal batteries. *Adv. Mater.* **2024**, *36*, e2314120. DOI
25. Liang, J.; Hwang, S.; Li, S.; et al. Stabilizing and understanding the interface between nickel-rich cathode and PEO-based electrolyte by lithium niobium oxide coating for high-performance all-solid-state batteries. *Nano. Energy.* **2020**, *78*, 105107. DOI
26. Wang, X.; Yushin, G. Chemical vapor deposition and atomic layer deposition for advanced lithium ion batteries and supercapacitors. *Energy Environ. Sci.* **2015**, *8*, 1889-904. DOI
27. Li, Z.; Su, J.; Wang, X. Atomic layer deposition in the development of supercapacitor and lithium-ion battery devices. *Carbon* **2021**, *179*, 299-326. DOI
28. Karimzadeh, S.; Safaei, B.; Yuan, C.; Jen, T. Emerging atomic layer deposition for the development of high-performance lithium-ion batteries. *Electrochem. Energy Rev.* **2023**, *6*, 192. DOI
29. Jung, Y. S.; Lu, P.; Cavanagh, A. S.; et al. Unexpected improved performance of ALD coated LiCoO_2 /graphite Li-ion batteries. *Adv. Energy Mater.* **2013**, *3*, 213-9. DOI
30. Han, X.; Gong, Y.; Fu, K. K.; et al. Negating interfacial impedance in garnet-based solid-state Li metal batteries. *Nat. Mater.* **2017**, *16*, 572-9. DOI
31. Qian, L.; Zheng, Y.; Or, T.; et al. Advanced material engineering to tailor nucleation and growth towards uniform deposition for anode-less lithium metal batteries. *Small* **2022**, *18*, e2205233. DOI
32. Li, Z.; Zheng, Y.; Liao, C.; et al. Advanced polymer materials for protecting lithium metal anodes of liquid-state and solid-state lithium batteries. *Adv. Funct. Mater.* **2024**, *34*, 2404427. DOI
33. Qian, H.; Li, X.; Chen, Q.; et al. $\text{LiZn/Li}_2\text{O}$ induced chemical confinement enabling dendrite-free Li-metal anode. *Adv. Funct. Mater.* **2024**, *34*, 2310143. DOI
34. Zhao, Y.; Zheng, K.; Sun, X. Addressing interfacial issues in liquid-based and solid-state batteries by atomic and molecular layer deposition. *Joule* **2018**, *2*, 2583-604. DOI
35. Chang, C.; Hu, S.; Li, T.; et al. A robust gradient solid electrolyte interphase enables fast Zn dissolution and deposition dynamics. *Energy Environ. Sci.* **2024**, *17*, 680-94. DOI
36. Yang, L.; Luo, D.; Zheng, Y.; et al. Heterogeneous nanodomain electrolytes for ultra-long-life all-solid-state lithium-metal batteries. *Adv. Funct. Mater.* **2022**, *32*, 2204778. DOI
37. Shi, J.; Nguyen, H.; Chen, Z.; et al. Nanostructured block copolymer single-ion conductors for low-temperature, high-voltage and fast charging lithium-metal batteries. *Energy Mater.* **2023**, *3*, 300036. DOI
38. Yang, X.; Huang, Y.; Li, J.; et al. Understanding of working mechanism of lithium difluoro(oxalato) borate in $\text{Li}||\text{NCM85}$ battery with enhanced cyclic stability. *Energy Mater.* **2023**, *3*, 300029. DOI
39. Zheng, Y.; Yang, N.; Gao, R.; et al. "Tree-trunk" design for flexible quasi-solid-state electrolytes with hierarchical ion-channels enabling ultralong-life lithium-metal batteries. *Adv. Mater.* **2022**, *34*, e2203417. DOI
40. Qiu, C.; Odarchenko, Y.; Meng, Q.; et al. Resolving the effect of oxygen vacancies on Co nanostructures using soft XAS/X-PEEM. *ACS Catal.* **2022**, *12*, 9125-34. DOI PubMed PMC
41. Oversteeg CH, Doan HQ, de Groot FM, Cuk T. In situ X-ray absorption spectroscopy of transition metal based water oxidation catalysts. *Chem. Soc. Rev.* **2017**, *46*, 102-25. DOI PubMed
42. Maugeri, L.; Simonelli, L.; Iadecola, A.; et al. Temperature dependent local structure of LiCoO_2 nanoparticles determined by Co

- K-edge X-ray absorption fine structure. *J. Power. Sources.* **2013**, *229*, 272-6. DOI
43. Ekwongsa, C.; Rujirawat, S.; Butnoi, P.; et al. Temperature dependent local structure of LiCoO₂ determined by in-situ Co K-edge X-ray absorption fine structure (EXAFS). *Radiat. Phys. Chem.* **2020**, *175*, 108545. DOI
 44. Croce, F.; Appetecchi, G. B.; Persi, L.; Scrosati, B. Nanocomposite polymer electrolytes for lithium batteries. *Nature* **1998**, *394*, 456-8. DOI
 45. Oyakhire, S. T.; Huang, W.; Wang, H.; et al. Revealing and elucidating ALD-derived control of lithium plating microstructure. *Adv. Energy. Mater.* **2020**, *10*, 2002736. DOI
 46. Wang, S.; Sun, Q.; Zhang, Q.; et al. Li-ion transfer mechanism of ambient-temperature solid polymer electrolyte toward lithium metal battery. *Adv. Energy. Mater.* **2023**, *13*, 2204036. DOI
 47. Mirsakiyeva, A.; Ebadi, M.; Araujo, C. M.; Brandell, D.; Broqvist, P.; Kullgren, J. Initial steps in PEO decomposition on a Li metal electrode. *J. Phys. Chem. C.* **2019**, *123*, 22851-7. DOI
 48. Lin, C.; Kozen, A. C.; Noked, M.; Liu, C.; Rubloff, G. W. ALD protection of Li-metal anode surfaces - quantifying and preventing chemical and electrochemical corrosion in organic solvent. *Adv. Mater. Inter.* **2016**, *3*, 1600426. DOI
 49. Li, B.; Su, Q.; Liu, C.; et al. Stable interface of a high-energy solid-state lithium metal battery via a sandwich composite polymer electrolyte. *J. Power. Sources.* **2021**, *496*, 229835. DOI
 50. Song, X.; Zhang, T.; Fan, R.; et al. A composite solid-state electrolyte of high ionic-conductivity garnet-type Li_{6.5}La₃Zr_{1.5}Ta_{0.1}Nb_{0.4}O₁₂ filler in PEO matrix. *Solid. State. Ion.* **2023**, *403*, 116410. DOI
 51. Liu, M.; Guan, X.; Liu, H.; et al. Composite solid electrolytes containing single-ion lithium polymer grafted garnet for dendrite-free, long-life all-solid-state lithium metal batteries. *Chem. Eng. J.* **2022**, *445*, 136436. DOI
 52. Yu, G.; Pan, L.; Zhang, H.; et al. Thin yet strong composite polymer electrolyte reinforced by nanofibrous membrane for flexible dendrite-free solid-state lithium metal batteries. *Adv. Energy. Sustain. Res.* **2022**, *3*, 2100193. DOI
 53. Moškon, J.; Gaberšček, M. Transmission line models for evaluation of impedance response of insertion battery electrodes and cells. *J. Power. Sources. Adv.* **2021**, *7*, 100047. DOI
 54. Ye, W.; Fan, Z.; Zhou, X.; Xue, Z. Functionalized polypropylene separator coated with polyether/polyester blend for high-performance lithium metal batteries. *Energy. Mater.* **2024**, *4*, 400049. DOI
 55. Groot FM, Grioni M, Fuggle JC, Ghijsen J, Sawatzky GA, Petersen H. Oxygen 1s X-ray-absorption edges of transition-metal oxides. *Phys. Rev. B. Condens. Matter.* **1989**, *40*, 5715-23. DOI PubMed
 56. Groot, F. D. Multiplet effects in X-ray spectroscopy. *Coordin. Chem. Rev.* **2005**, *249*, 31-63. DOI
 57. Li, F.; Li, Y.; Chen, H.; et al. Impact of strain-induced changes in defect chemistry on catalytic activity of Nd₂NiO_{4+δ} electrodes. *ACS. Appl. Mater. Interfaces.* **2018**, *10*, 36926-32. DOI
 58. Huang, R.; Ding, Y.; Zhang, F.; et al. The interphasial degradation of 4.2 V-class poly(ethylene oxide)-based solid batteries beyond electrochemical voltage limit. *J. Energy. Chem.* **2022**, *75*, 504-11. DOI
 59. Kim, D. S.; Kim, Y. E.; Kim, H. Improved fast charging capability of graphite anodes via amorphous Al₂O₃ coating for high power lithium ion batteries. *J. Power. Sources.* **2019**, *422*, 18-24. DOI
 60. Zhang, H.; Xu, Z.; Shi, B.; et al. Enhanced cyclability of Cr₈O₂₁ cathode for PEO-based all-solid-state lithium-ion batteries by atomic layer deposition of Al₂O₃. *Materials* **2021**, *14*, 5380. DOI PubMed PMC
 61. Hyun, D.; Jung, Y.; Kim, T.; et al. Multi-functional Al₂O₃-coated separators for high-performance lithium-ion batteries: critical effects of particle shape. *Ceram. Int.* **2023**, *49*, 30147-55. DOI